Application of X-ray Absorption Fine Structure (XAFS) to Local-Order Analysis in Fe-Cr Maghemite-like Materials

E. Montero-Cabrera, L. E. Fuentes-Cobas, E. Macías-Ríos, M. E. Fuentes-Montero

Abstract

The maghemite-like oxide system ψ-$Fe_{2-x}Cr_xO_3$ (x=0.75, 1 and 1.25) was studied by X-ray absorption fine structure (XAFS) and by synchrotron radiation X-ray diffraction (XRD). Measurements were performed at the Stanford Synchrotron Radiation Lightsource at room temperature, at beamlines 2-1, 2-3 and 4-3. High-resolution XRD patterns were processed by means of the Rietveld method. In cases of atoms being neighbors in the Periodic Table, the order/disorder degree of the considered solutions is indiscernible by “normal” (absence of “anomalous scattering”) diffraction experiments. Thus, maghemite-like materials were investigated by XAFS in both Fe and Cr K-edges to clarify, via short-range structure characterization, the local ordering of the investigated system. Athena and Artemis graphic user interfaces for IFEFFIT and FEFF8.4 codes were employed for XAFS spectra interpretation. Pre-edge decomposition and theoretical modeling of X-ray absorption near edge structure (XANES) transitions were performed. By analysis of the Cr K-edge XANES, it has been confirmed that Cr is located in an octahedral environment. Fitting of the extended X-ray absorption fine structure (EXAFS) spectra was performed under the consideration that the central atom of Fe is allowed to occupy octa- and tetrahedral positions, while Cr occupies only octahedral ones. Coordination number of neighboring atoms, interatomic distances and their

quadratic deviation average were determined for x=1, by fitting simultaneously the EXAFS spectra of both Fe and Cr K- edges. The results of fitting the experimental spectra with theoretical standards showed that the cation vacancies tend to follow a regular pattern within the structure of the iron-chromium maghemite ($FeCrO_3$).

X-ray absorption fine structure (XAFS) techniques allow understanding the crystalline and electronic structure of the nearest neighbors of an atom under study. XAFS studies about oxidation states, interatomic distances and other properties display some advantages, as the measurement of the X-ray absorption coefficient energy dependence allows to perfectly distinguish neighboring elements in the Periodic Table. XAFS stands for the observed modulation in the x- rays absorption coefficient in energies near and above the absorption edge in an element of a material. Conventionally, the observed effects are divided in two regions, X-ray absorption near edge structure (XANES) and the Extended X-ray absorption fine structure (EXAFS). XANES offers information on oxidation state of the absorbing element. EXAFS allows the determination of distances, coordination numbers and species of the first neighbors of the absorbing atom. Both spectroscopies offer information on the local atomic coordination from distances normally of 0.5 nm to 0.8 nm. XAFS experiments require x-rays sources of high intensity and tunable energies, as it is the case of synchrotron radiation (SR).

XAFS correct interpretation and its experimental implementation were made from the works of Stern, Lytle and Sayers [1-4].

In order to focus in the oscillations of the absorption coefficient μ(E) depending on the energy, the EXAFS function is defined [3, 5] by

$$\chi(E)=\frac{\mu(E)-\mu_0(E)}{\Delta\mu_0(E)},$$

where $\mu_0(E)$, the smooth function of background of the bare atom, has been subtracted from $\mu(E)$ and the result has been divided by the height of the absorption edge, to normalize the absorption event to 1. To extract information of the EXAFS spectrum it is used the so-called "EXAFS equation" [2].

The EXAFS spectra are interpreted by modelling a proposed structure, with programs developed to the effect, such as FEFF [6], EXCURV [7] and GNXAS [8, 9]. For that modelling a great amount of information is used from the system in study, to calculate the values of *F(k)* and *δ(k)* (the amplitude and phase shift of the wave of the scattered photoelectron—both quantities reflect the properties of *neighboring atoms* when scattering the photoelectron) of the different coordination spheres. With those functions the contribution of each sphere of the model to the spectrum is calculated and the values of *N, R* and σ^2 of each coordination sphere are refined (R_j being the distance to neighboring atoms, N_j – the coordination number of neighboring atoms and σ_j –the quadratic deviation average of the distance to the neighbors).

The objective of the present article is to show how the application of XAFS techniques has allowed the identification of unresolved by XRD attributes of the crystalline structure. The study consisted on the examination of XANES features in transition metals and on EXAFS fitting of *N, R* and σ^2 for the ψ-$Fe_{2-x}Cr_xO_3$ maghemite (x=0.75, 1 and 1.25) dual oxide system.

Materials and Methods

Characteristics and preparation of γ−$Fe_{2-x}Cr_xO_3$

Ferrimagnetic maghemite-like materials as ψ-$Fe_{2-x}Cr_xO_3$ (*x*=0.75, 1 and 1.25) have been prepared by the so-called solution-combustion synthesis [10]. Figure 1 schematically shows the spinel structure of the studied maghemite-like materials, in the following called simply *maghemites*. An important open question is the distribution of Fe, Cr and vacancies among the octahedral and tetrahedral spinel sites. Concerning vacancies, for the case of pure maghemite γ−Fe_2O_3; Shmakov et al. [11] propose they are located on the 4b octahedral sites of the $P4_332$ space group, while Jorgensen et al. [12] suggest they are distributed among tetrahedral and octahedral sites of Fd−3m. Regarding Fe and

Cr, it is reasonable to expect that Cr^{+3}, as a $t_{2g}^{\ 3}$ cation, with few exceptions [13, 14], should go to octahedral positions, while Fe^{+3}, a $t_{2g}^{\ 3}e_g^{\ 2}$ cation in a high spin configuration, would be in either octahedral or tetrahedral positions.

Considered maghemites were studied by X-ray absorption fine structure (XAFS) of the K-absorption edge of two elements and by synchrotron radiation high-resolution X-ray diffraction (XRD). Double-element XAFS analysis was applied to clarify the local configuration of maghemite systems. XAFS would confirm or reject the random character of the solution, among other features. XRD and XAFS measurements were performed at the Stanford Synchrotron Radiation Lightsource (SSRL) at room temperature.

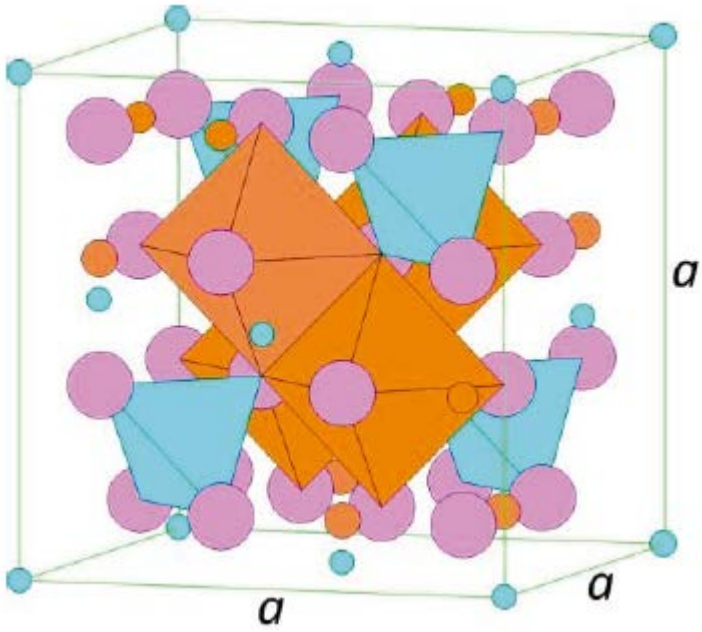

FIGURE 1. Spinel structure of ψ-$Fe_{2-x}Cr_xO_3$ (x=0.75, 1 and 1.25). Magenta spheres represent oxygen atoms; coordination tetrahedra and octahedra around cations are respectively blue and pumpkin.

Diffraction peaks provide information about long-range (global, average) order and diffuse scattering informs about short-range (local) order-disorder phenomena [15]. XAFS is the spectroscopic variant for short-range order-disorder investigation. Each technique has its special value. For example, in the determination of the pair distribution function XAFS is element-sensitive and diffuse scattering is not. In the present work we have characterized global order by diffraction and local ordering by means of XAFS. The results of both analyses are consistent and complementary

XAFS Attributes for Transition Metals Study

XANES analysis provides the possible identification of particular

photoelectron transitions. This is the case when analyzing the main absorption "jump" and the so-called *pre-edge features* of the absorption edge function on energy. The energies of the valence orbitals and, accordingly, the energy position of the edge and pre-edge features are linked with the oxidation state of transition metals in the sample. Each absorption feature is shifted to higher energies as the oxidation state increases. The largest shifts, which are up to a few electron volts per oxidation "unity", are observed at the edge position, which may be identified by the inflection point in the absorption edge function. The *pre-edge* region of the spectra before the K-edge jump contains peaks, explained by electronic transitions to unoccupied bound states located below the vacuum level. One prominent peak exists as a result of the photoelectron transitions $1s \nrightarrow 3d$. These dipolar transitions in the transition metals are prohibited because $\Delta l = 2$ and the metal atoms are in a very symmetrical environment, when a metal cation occupies an octahedral site. In the case of tetrahedral or distorted octahedral geometries of increasing oxidation states, bonds of *3d* state mixed with the *2p* ligand oxygen are formed and an intensifying dipole transition is possible. Detecting and analyzing the pre-edge features allows recognizing the transition metal cations oxidation state and/or occupancy of particular sites in the local structure.

In the present investigation of compounds containing Cr and Fe cations, the study of the mentioned attributes of the XANES spectra provide key information about oxidation states and local environment. For the maghemite system ψ- $Fe_{2-x}Cr_xO_3$, X-ray diffraction reports the positions for the "Cr-Fe average atom" and the oxygen. EXAFS, for Cr or Fe as absorbents, provides Fe-O, Cr-O, Cr-Fe, Fe-Fe, and

Cr-Cr distances. The analysis of the first inflection shifts at about the energy of the main jump, calculated as the difference between its position in the pure transition metal (zero oxidation) and the corresponding position of the studied substance, as well as the study of above mentioned pre-edge features, are considered for the subsequent EXAFS analysis.

Synchrotron Radiation Experiments

The global structures of the studied materials were investigated by high-resolution X-ray powder diffraction. At SSRL beamline 2-1, the samples were mounted on a zero background holder and data were collected in reflection geometry at 12 keV (λ = 1.03265Å) from 10° to 110° in 2θ. The instrumental resolution was calibrated with a standard LaB_6 sample. The experimental data were processed by Fullprof program [16], using microstructural characterization routine to estimate the crystallite size and heterogeneous deformations of the lattice parameters. The scanning step was 0.01◦ in 2θ.

Oxide samples were investigated by XAFS on Fe and Cr K-edges. Measurements were performed at the SSRL at room temperature, at beamlines 2-3 and 4-3, in fluorescence mode, using Lytle + ion-chamber detectors. The SPEAR-3 storage ring was operated at 3.0 GeV with a beam current of 100 mA. Absorption coefficient measurements were performed using a pure metal reference between I_1 and I_2 chambers, with Mn filter in the Lytle detector for the case of Fe K-edge. For Cr K-edge, a V filter in the Lytle was employed. Data were recorded on both XANES and EXAFS regions. $Cr(III)_2O_3$ (corundum), $Cr(IV)O_2$ (rutile) and $SrCr(VI)O_4$ were used as model compounds for Cr K-edge features comparison, when necessary.

Athena and Artemis codes as interfaces for IFEFFIT [17] and FEFF8.4 [18] codes were employed for XAFS spectra interpretation. Pre-edge decomposition and theoretical modeling of X-ray absorption near edge structure (XANES) transitions were performed. In the study of maghemite, interatomic distances were determined by the fitting of average spectra in the Extended X-ray

absorption fine structure (EXAFS) region in both edges simultaneously.

Results and Discussion

X-Ray Diffraction

Figure 2 shows the XRD patterns from samples □-Fe2-*x*Cr*x*O3, with nominal compositions (*x* = 0.75, 1.00, 1.25).The inset shows a zoom of the 440 peak in the three samples tested. The observed peaks' broadening and asymmetry is representative for the collected spectra. The peaks of the "*stoichiometric*" *x* = 1 sample (□-FeCrO3) are sharp and correspond to the minimum lattice parameter of the investigation. For both *x* < 1 and *x* > 1, the lattice parameter increases and peaks broaden. Forbidden (superlattice) reflections were not observed. The XRD peak broadening is primarily associated with an inhomogeneity in the dimensions of the unit cells produced by spatial variations in the amount and distribution of Cr+3 and Fe+3 cations and vacancies.

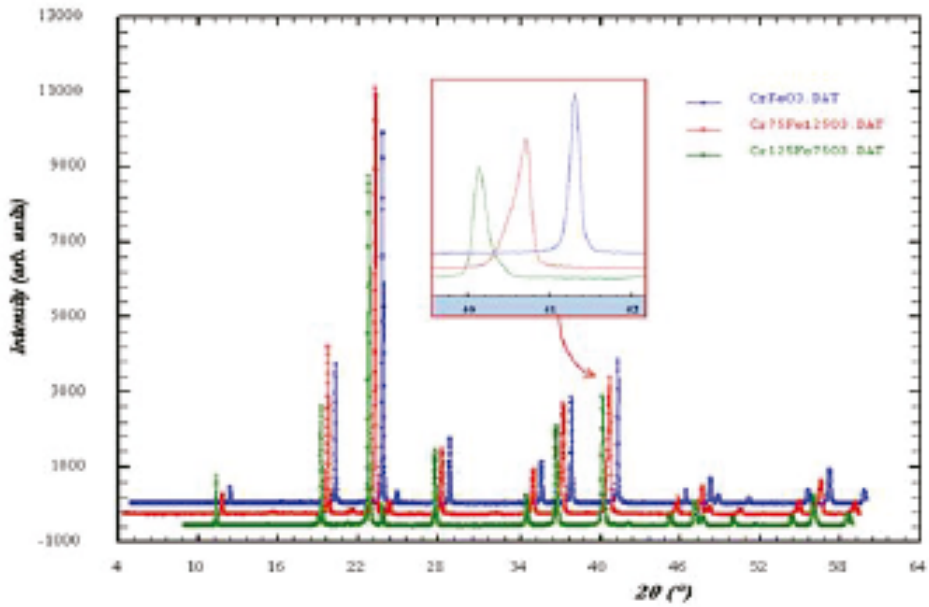

FIGURE 2: XRD of ψ-$Fe_{2-x}Cr_xO_3$ samples with (x = 0.75, 1.00, 1.25).

Atomic parameters						
Atom	x(σ_x)	Y(σ_y)	Z(σ_z)	B(σ_B)	Occ. (σ_{occ})	Multiplicity (site)
O	0.2573(3)	0.2573(3)	0.2573(3)	0.65(9)	32	32
Fe	0.1250	0.1250	0.1250	0.56(6)	7.76(3)	8 (tetrahedral)
Fe	0.5000	0.5000	0.5000	0.44(5)	2.90(3)	16 (octahedral)
Cr					10.66667	

TABLE 1: The structure of ψ-$FeCrO_3$.

Space group Fd -3m, lattice parameter α = 8.2881 (1) Å.

The peak broadening analysis led to the following microstructural results: Average crystallite size: 758.4 (3) Å

Average micro-strain: 11.38 (5) %% (parts in ten thousands)

Research on the distribution of Fe^{3+} cations between tetra- and octahedral sites led to interesting results given in Table 1: About 3% (= 0.24/8) vacancies are in tetrahedral sites. This result is consistent with that reported by Jorgensen [12] for pure iron maghemite and represents a subtle difference to the approximate model proposed by Grau-Crespo et al. [19].

Consideration of the x = 0.75 and 1.25 samples, taking into account the asymmetric peaks' broadening represented by the inset of Figure 2, leads to the conclusion that these samples are formed by heterogeneous distributions of continuously varying micro-structures, presumably associated with compositional inhomogeneity. This result prevents a reliable characterization of their ordering condition by diffraction.

X-ray Absorption Fine Structure

By comparison with measurements of oxidation states on model compounds Cr_3O_2

(corundum-III), and CrO_2 (rutile-IV), performed in the same session, it was possible to confirm the Cr^{+3} oxidation state in O_h environment at the $\gamma-Fe_{2-x}Cr_xO_3$ compounds [20-22]. Computation of theoretical XANES spectrum using FEFF8.4 [18] of $\gamma-FeCrO_3$ for one model configuration, considering a simple distribution of vacancies and Cr in octahedral sites, is presented in part

a) of Figure 3. Both results strongly suggest the Cr^{+3} character of this ion in study samples, as well as their octahedral occupation. Figure 3 c) shows the general view of obtained Cr K-edge XANES spectra.

The study of Fe^{+3} in octahedral and tetrahedral sites using XANES spectra was performed also by both pre-edge decomposition [23] and theoretical modeling via FEFF8.4 [18]. Experimental XANES spectra are very similar to those, reported in XANES studies of ψ-Fe_2O_3 [23-25]. Pre-edge analysis information practically coincide with the results presented in [23] for natural maghemite. In the theoretical modeling of XANES Fe K-edge spectra, (Fe-Cr) shared octahedral positions are fully occupied by Cr and five nonequivalent vacancy configurations, for X-rays diffraction almost doesn't notice differences between close atomic number elements as Cr and Fe. Vacancies were described by null occupancies. Weighted average by relative population of different configurations of obtained model results is presented in Figure 3 b). All the features of the XANES experimental spectra are reproduced by the model; therefore it can be considered a successful one. Both pre-edge analysis and theoretical modelling strongly support the XRD results presented above.

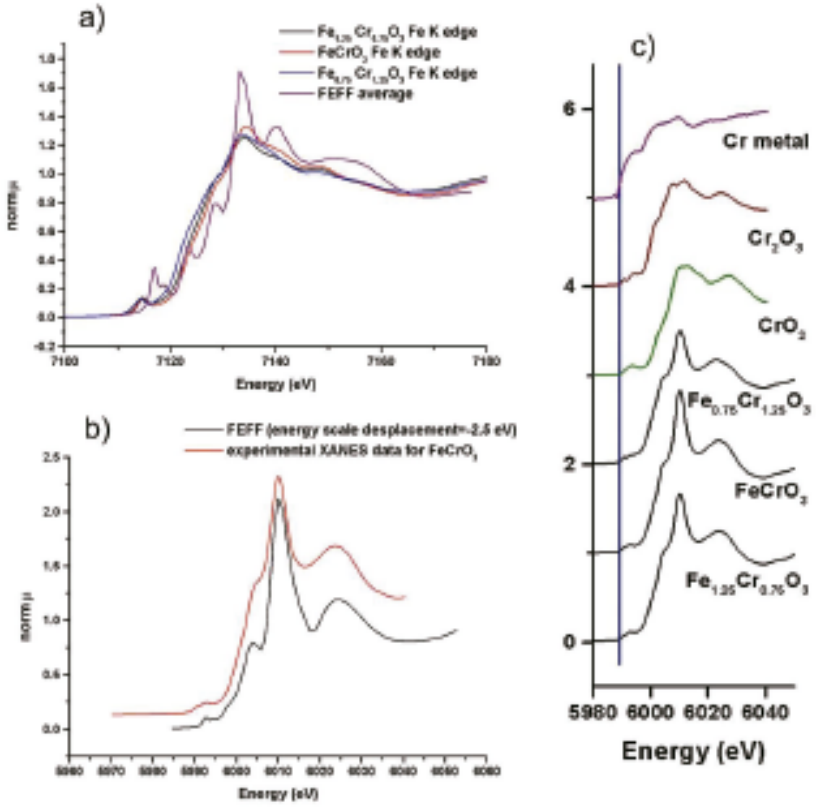

FIGURE 3. XANES of maghemites. a) Comparison of FEFF theoretical average for octahedral and tetrahedral iron absorbing sites and experimental γ−$FeCrO_3$ Fe K-edge XANES spectra of γ−$FeCrO_3$. The theoretical doublet at 7118-19 eV was also detected in close observation of experimental pre-edges features. b) Comparison of FEFF theoretical and experimental Cr K-edge XANES spectra of γ−$FeCrO_3$. For both Fe and Cr K-edges, it may be noticed that all features of experimental spectra have the corresponding signal in the FEFF8.4 theoretical spectra. c) Comparison of XANES Cr K edge spectra of γ−$FeCrO_3$ and model compounds. The first inflection of the main edge in maghemite samples are at 5998.2, 5999.4 and 5998.8 eV, for Cr contents x = 0.75, 1.00 and 1.25, respectively; and Cr_2O_3 and CrO_2 are at 5999.4 and 6001.3 eV, respectively. Also, the pre-edge peak is practically vanishing in maghemite spectra. N, R and σ^2 structural parameters were determined for x=1, by the fitting of average spectra in the EXAFS region in both edges simultaneously. The results of XANES analysis about occupancy of Fe^{3+} and Cr^{3+} required fitting the EXAFS spectra with the central absorbing atom of Fe being able to occupy both tetrahedral and octahedral positions, together with Cr absorbing atoms occupying only the octahedral sites. As XRD patterns do not show any super- structural peaks, meaning that the long-range order in the iron-chromium maghemite (ψ-$FeCrO_3$) is cubic, the examination of order at local scale is required.

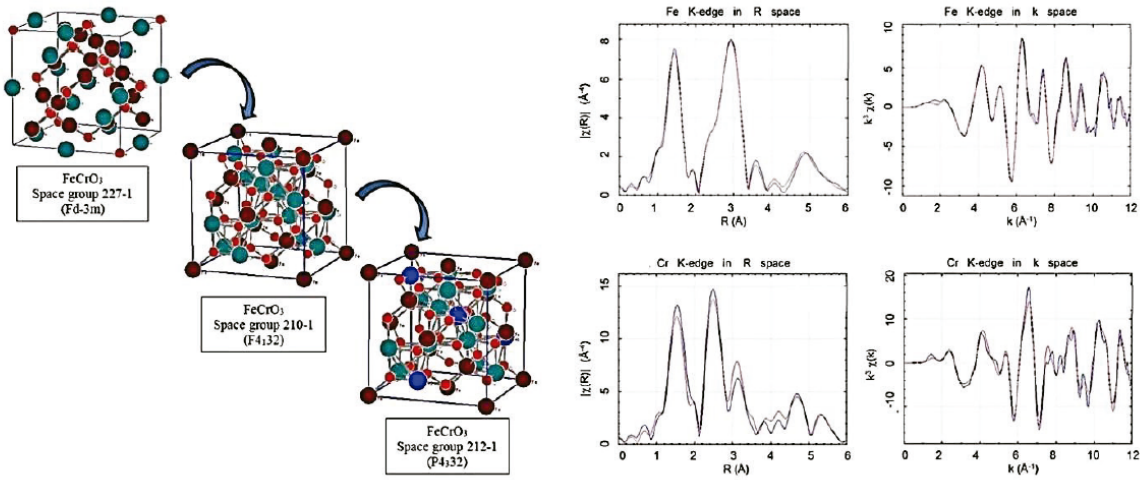

FIGURE 4. Left: Models for EXAFS interpretation and vacancies occupation. Octahedral sites L1, L4, L7 and L10 at Wyckoff 4b sites, shown in blue, are always occupied by either Cr^{3+} or Fe^{3+}. Right: Final fitting of experimental EXAFS spectra with theoretical standards corresponding to octahedral sites L1, L4, L7 and L10 always occupied by either Cr^{3+} or Fe^{3+}.

Grau-Crespo et al. in [19] provided theoretical arguments about a favorable electrostatic contribution of Fe^{+3} cations in the pure iron maghemite, with an *ordered supercell* configuration based on the $P4_332$ cubic structure that exhibits the maximum possible homogeneity in the distribution of iron cations and vacancies. In the EXAFS theoretical modelling of experimental Fe and Cr K-edges spectra simultaneously, fitting of successive coordination distances up to Å, coordination number of neighboring atoms and site occupancies-vacancies were strategically being constrained to check the correctness of the model of disordered or ordered vacancies in the octahedral sites as a trend in the *local order* of the maghemite ψ-$FeCrO_3$. The first model consisted on “gray” occupation of Fe^{3+}-vacancy or Cr^{3+}-vacancy at any octahedral site. The second model consisted on a “gray” cation, occupying the Wyckoff 4b sites of the symmetry $P4_332$. The final step considers that the cation vacancies tend to be located orderly within the structure of the iron-

chromium maghemite (ψ-$FeCrO_3$) at Wyckoff 4b sites L2, L3, L5, L6, L8, L9, L11 and L12, given on right of Figure 4 [19]. This model constrains all vacancies in octahedral sites, giving 16.6 % as open sites. The XRD results given above provide some vacancies located in tetrahedral sites, and only 15.2 % of vacancies in octahedral sites. When successive models were introduced, the R factor of the fitting was improved from 0.009 to 0.004, while other parameters of fitting were improved in five times. The successive fitted structures are shown in the left part of Figure 4. The results of fitting the experimental EXAFS spectra with theoretical standards are given in the right part of Figure 4.

CONCLUSIONS

The study of chromium maghemites ψ-$Fe_{2-x}Cr_xO_3$ in the vicinity of x = 1, using high resolution diffraction and XANES on a synchrotron light source, has allowed the characterization of the oxidation states and the crystal structure at local and global levels.

Globally, by XRD, it has been found that the symmetrical composition x = 1 produces the most uniform and unstrained samples. Chromium ions occupy only octahedral sites, while iron occupies octa- and tetrahedral positions. Vacancies are located mostly in octahedral sites, with a small but detectable proportion of tetrahedral locations.

For the case of the symmetrical composition of the Fe-Cr maghemites, both pre-edge analysis and theoretical modelling by FEFF 8.4 code of XANES spectra for Fe- and Cr- K edges strongly support the XRD results. The results of fitting the experimental EXAFS spectra with theoretical standards obtained by the FEFF 8.4

code showed that the maghemite cation vacancies tend to follow a regular pattern within the structure, as the model suggested by Grau- Crespo et al.

ACKNOWLEDGMENTS

Portions of this research were carried out at the Stanford Synchrotron Radiation Laboratory, a national user facility operated by Stanford University on behalf of the U.S. Department of Energy, Office of Basic Energy Sciences. The SSRL Structural Molecular Biology Program is supported by the Department of Energy, Office of Biological and Environmental Research, and by the National Institutes of Health, National Center for Research Resources, Biomedical Technology Program. The oxides' synthesis was performed at Departamento de Química Inorgánica I, Facultad de Ciencias Químicas, Universidad Complutense de Madrid. Funds from Consejo Nacional de Ciencia y Tecnología of Mexico, Projects CONACYT 46515 and CONACYT-CNPQ 174391 are gratefully acknowledged. M E Montero Cabrera wishes to thank Joshua Kas for his help in FEFF calculations.

REFERENCES

1. F. W. Lytle, D. E. Sayers and E. A. Stern, Phys. Rev. B **11** (12), 4825-4835 (1975).
2. D. E. Sayers, E. A. Stern and F. W. Lytle, Phys. Rev. Lett. **27** (18), 1204-1207 (1971). 3. E. A. Stern, Phys. Rev. B **10** (8), 3027-3037 (1974).
3. E. A. Stern, D. E. Sayers and F. W. Lytle, Phys. Rev. B **11** (12), 4836-4846 (1975).
4. D. C. Koningsberger and R. e. Prins, *X-ray absorption: principles, applications, techniques of EXAFS, SEXAFS, and XANES*. (John Wiley and Sons, New York, NY, United States, 1988).

5. J. J. Rehr and R. C. Albers, Rev. Mod. Phys. **72** (3), 621-654 (2000).
6. N. Binsted and S. S. Hasnain, Journal of Synchrotron Radiation **3**, 185-196 (1996). 8. A. Filipponi and A. DiCicco, Phys. Rev. B **52** (21), 15135-15149 (1995).
7. A Filipponi, A. DiCicco and C. R. Natoli, Phys. Rev. B **52** (21), 15122-15134 (1995).
8. M. Garcia-Guaderrama, M. A. Alario-Franco, O. Blanco and E. Moran, in *Solid-State Chemistry of Inorganic Materials VII* (Cambridge University Press (CUP) / Materials Research Society (MRS), Boston, Massachusetts, USA, 2008), Vol. 1148, pp. 137-142.
9. A N. Shmakov, G. N. Kryukova, S. V. Tsybulya, A. L. Chuvilin and L. P. Solovyeva, J. Appl. Crystallogr. **28** (2), 141-145 (1995).
10. J.-E. Jorgensen, L. Mosegaard, L. E. Thomsen, T. R. Jensen and J. C. Hanson, J. Solid State Chem. **180** (1), 180-185 (2007).
11. C. K. Jørgensen, *Inorganic Complexes*. (Academic Press, London-New York 1963).
12. N. Gorodylova, V. Kosinova, P. Sulcova, P. Belina and M. Vlcek, Dalton Transactions **43** (41), 15439-15449 (2014).
13. T. R. Welberry, *Diffuse X-Ray Scattering and Models of Disorder*. (Paperback: Thomas - Oxford University Press, Oxford, UK, 2010).
14. J. Rodríguez-Carvajal, Commission on Powder Diffraction Newsletter **26**, 12–19 (2001).
15. B. Ravel and M. Newville, Journal of Synchrotron Radiation **12** (4), 537-541 (2005).
16. A L. Ankudinov, B. Ravel, J. J. Rehr and S. D. Conradson, Phys. Rev. B **58**

(12), 7565-7576 (1998).

17. R. Grau-Crespo, A. Y. Al-Baitai, I. Saadoune and N. H. De Leeuw, J. Phys.: Condens. Matter **22**, 255401 (2010).
18. H. Bea, M. Bibes, S. Fusil, K. Bouzehouane, E. Jacquet, K. Rode, P. Bencok and A. Barthelemy, Phys. Rev. B **74** (2), 4 (2006).
19. A Pantelouris, H. Modrow, M. Pantelouris, J. Hormes and D. Reinen, Chem. Phys. **300** (1-3), 13-22 (2004).
20. Arcon, B. Mirtic and A. Kodre, J. Am. Ceram. Soc. **81** (1), 222-224 (1998).
21. M. Wilke, F. Farges, P. E. Petit, G. E. Brown and F. Martin, Am. Mineral. **86** (5-6), 714-730 (2001).
22. P. A. O'Day, J. J. Rehr, S. I. Zabinsky and G. E. Brown, Jr., J. Am. Chem. Soc. **116** (7), 2938- 2949 (1994).
23. T. C. Rojas, J. C. Sanchez-Lopez, J. M. Greneche, A. Conde and A. Fernandez, Journal of Materials Science **39** (15), 4877-4885 (2004).